Science Advances
AAAS

advances.sciencemag.org/cgi/content/full/5/11/eaay2748/DC1

Supplementary Materials for

Entropic elasticity and negative thermal expansion in a simple cubic crystal

David Wendt, Emil Bozin, Joerg Neuefeind, Katharine Page, Wei Ku, Limin Wang, Brent Fultz, Alexei V. Tkachenko, Igor A. Zaliznyak*

*Corresponding author. Email: zaliznyak@bnl.gov

Published 1 November 2019, *Sci. Adv.* **5**, eaay2748 (2019)
DOI: 10.1126/sciadv.aay2748

This PDF file includes:

Supplementary Text

Crystal structure and structural phase transition in ScF_3

ScF_3 crystallizes in a simple AMX_3 cubic perovskite structure (P*m*3*m*) with the A cations absent[10,12] (the ReO_3 structure[36,37]). Sc plays the role of the M cation and is surrounded by a corner-sharing octahedron of fluorine atoms (Fig. 1A). Unlike its relative, α-AlF_3, which undergoes a transition to the low-temperature rhombohedral phase at about 730 K (this symmetry reduction can be viewed as a rotation of fluorine octahedra about the cubic diagonal direction; adjacent octahedra rotate in the opposite sense, and thus the wave vector of this distortion is (0.5,0.5,0.5) and the unit cell is doubled)[37], at ambient pressure ScF_3 remains cubic down to $T < 1$ K[38]. The rhombohedral distortion was found to appear in ScF_3 under pressure[9,18,38], with the transition temperature to the cubic phase decreasing roughly linearly, from about 300 K at 0.7 GPa to near zero at $P = 0$. Similarly, distorted phase appears with Sc substitution by Y in $(Sc)_{1-x}Y_xF_3$, where the transition temperature increases with doping, x[18,38]. The stoichiometric, ScF_3 material shows anomalous non-Debye heat capacity at low T, indicating failure of the conventional Debye phonon description[38].

These remarkable observations suggest that ScF_3 exists in very close proximity to a $T = 0$ structural quantum phase transition (QPT) where the energies of the two competing phases are nearly equal[18]. In such situation, the low-energy properties that define lattice stability and thermal expansion often cannot be described using harmonic oscillator approximation based on either of the competing structures and new physics emerges governing the system's behavior. This is not dissimilar to QPT in a spin system of correlated electron materials, where quantum fluctuations often lead to new ground states and excitations. Instead of acquiring magnetic order, the system remains a correlated paramagnet (in some cases identified as spin liquid) down to $T = 0$ and it is the emergent local correlation patterns imposed by quantum fluctuations rather than phonon-like collective harmonic oscillator modes that govern the system's properties.

While these structural details and correlated atomic motions preserving local structural arrangements, such as RUM are important for understanding the low-temperature behavior and structural phase transition in ScF_3 and related materials, here we show that they are only a sub-leading effect for negative thermal expansion. The entropic elasticity origin of NTE has its roots in thermal fluctuations, which are only weakly sensitive to fine quantum effects that dominate the low-temperature behavior.

Supplementary Theory

Entropic elasticity and NTE in the floppy network model of ScF_3

We first consider a simple model of the ScF_3 lattice illustrated in Figure 3 of the main text, where all Sc-F bonds are replaced with rigid monomer links of length r_b and Coulomb interaction acts between all other pairs of ions. The rigid Sc-F link constraint represents the cumulative effect of all interactions acting between the nearest neighbors: electrostatic Coulomb attraction and core repulsion, as well as contribution from covalent bonding. The resulting Hamiltonian of the system has a simple form

$$H = K + \frac{1}{2}\sum_{i,j\ (r_{ij}>r_b)} V_{ij} = K + \frac{1}{2}\sum_{i,j\ (r_{ij}>r_b)} \frac{Z_i Z_j e^2}{4\pi\varepsilon_0 r_{ij}}. \quad \text{(S1)}$$

Here, K is kinetic energy, V_{ij} is potential energy of electrostatic Coulomb interaction between the two ions with indices i and j separated by distance r_{ij}, which we treat here as point charges, $Z_i e$ and $Z_j e$, respectively, e is electron charge and ε_0 is the vacuum permittivity (1/2 accounts for double counting of each pair in the sum). Without electrostatics, the network is under-constrained (floppy): the number of constraints imposed by rigid Sc-F links is 6 per unit cell, while the number of degrees of freedom is 12. In particular, the motion of Sc ion is constrained by rigid bonds in all 3 directions while each of F ions has two zero-energy displacement modes corresponding to motion orthogonal to Sc-F bond. The situation is similar to that of a freely jointed polymer chain

and in the absence of external tension the system would have no rigidity and would collapse. In ScF_3, Coulomb repulsion between the charged ions provides tension (negative pressure), which stabilizes the system and balances its entropic elasticity[2,3,39].

We thus start by considering a very simple mean field (MF) version of the model in which entropic elasticity of the floppy network of rigid Sc-F links balances the net electrostatic Coulomb repulsion between the like-charged ions (i. e. the sum of all Coulomb interactions excluding the attractive contribution of the nearest Sc-F pairs). The corresponding part of the free energy of the system can be written as

$$F = 3N\left[-k_B T \ln[\langle \vec{u}_\perp^2 \rangle] + \frac{(6-M)e^2}{4\pi\varepsilon_0 r} - \frac{\gamma e^2}{4\pi\varepsilon_0 r^3}\frac{\langle \vec{u}_\perp^2 \rangle}{2}\right] \quad \text{(S2)}$$

Here, N is the number of unit cells in the crystal, k_B is the Boltzmann constant, and $r = a/2$ is half the lattice constant, i.e. half of the average distance between the nearest Sc ions. The first term represents entropic contribution associated with the floppy modes, with $\vec{u}_\perp$ being the displacement of F ion in the direction perpendicular to the Sc-F bond and $\langle \vec{u}_\perp^2 \rangle$ thermal average of its square. The second term corresponds to the Coulomb contribution to the lattice energy assuming that all ions are at their nominal positions (Madelung energy), $U_M = \sum_{i,j} \frac{Z_i Z_j e^2}{4\pi\varepsilon_0 r_{ij}} = M\frac{e^2}{4\pi\varepsilon_0 r}$, minus the nearest-neighbor Sc-F Coulomb interactions. $M \approx 2.98$ is the Madelung constant for ScF_6 lattice[40,41], which can be straightforwardly computed using the method of Evjen[42]. The third term in Eq. (S2) accounts for the correction to electrostatic energy resulting from the average displacement of the F ions from their nominal lattice positions due to fluctuations. It was found in the MF approximation by calculating the change in point charge electrostatic energy following the displacement of a single F ion normal to the nominal direction of Sc-F bond, by the amount $\vec{u}_\perp$

$$\delta U_M(\vec{u}_\perp) = \sum_{n,r_n>r_0} \frac{Z_n e^2(1-3(\hat{a}\cdot\hat{r}_n)^2)}{4\pi\varepsilon_0 r_n^3}\frac{\vec{u}_\perp^2}{2} = -\frac{\gamma e^2}{4\pi\varepsilon_0 r^3}\frac{\vec{u}_\perp^2}{2} \quad \text{(S3)}$$

Here, $\hat{a}$ is the unit lattice vector along the nominal direction of the Sc-F bond, $\vec{r}_n$ is the position of the n-th site in the lattice with respect to the displaced F ion, $r_n = |\vec{r}_n|$, and $\hat{r}_n = \vec{r}_n/r_n$. The numerical factor, $\gamma \approx 0.9$, was obtained by numerical summation, in the same way as Madelung constant, M. Note that this correction term in the Hamiltonian is negative, which means that if favors transverse displacement of F ions and corresponds to making the floppy modes more unstable.

Both r and $\langle\vec{u}_\perp^2\rangle$ depend on temperature and should be obtained via minimization of the free energy, Eq. (S2). In our model, the free energy is minimized under the rigid Sc-F bond constraint, which imposes the relation between $\langle\vec{u}_\perp^2\rangle$ and r^2 following from the Pythagorean theorem

$$r^2 + \langle\vec{u}_\perp^2\rangle = r_b^2, \text{ or, for small } \langle\vec{u}_\perp^2\rangle \ll r_b^2,\ r \approx r_b - \frac{\langle\vec{u}_\perp^2\rangle}{2r_b} \quad \text{(S4)}$$

Substituting this constraint into Eq. (S3) we obtain

$$F = 3N\left[-k_B T \ln(r_b^2 - r^2) + \frac{(6-M)e^2}{4\pi\varepsilon_0 r} - \frac{\gamma e^2}{4\pi\varepsilon_0 r^3}\frac{(r_b^2 - r^2)}{2}\right] \quad \text{(S5)}$$

In the leading order, this expression can be linearized in $|r_b - r|/r_b \ll 1$ (or, the constraint can be expanded to leading order in $\langle\vec{u}_\perp^2\rangle/r_b^2 \ll 1$, $r \approx r_b - \frac{\langle\vec{u}_\perp^2\rangle}{2r_b}$), resulting in

$$F = 3N\left[-k_B T \ln(r_b - r) + \frac{(6-M)e^2}{4\pi\varepsilon_0 r} - \frac{\gamma e^2 (r_b - r)}{4\pi\varepsilon_0 r_b^2}\right] + O\left(\left(\frac{r_b - r}{r_b}\right)^2\right) \quad \text{(S6)}$$

By minimizing this free energy with respect to r, we obtain a Negative Thermal Expansion effect

$$\frac{r - r_b}{r_b} = -\frac{4\pi\varepsilon_0 r_b}{(6-M-\gamma)e^2} k_B T = \alpha_0 T \quad , \quad \alpha_0 = -\frac{4\pi\varepsilon_0 r_b k_B}{(6-M-\gamma)e^2} \approx -5.7 \cdot 10^{-6} K^{-1} \quad \text{(S7)}$$

Although in deriving Eq. (S7) we have neglected the important effects of ionic polarizability and the finite rigidity of Sc-F bond, which we consider below, this result compares favorably with the measured NTE in ScF_3, where the near room temperature NTE of ≈ -7.5 ppm/K is observed (Figs 2 and 4 of the main text)[7,9].

Effect of ionic polarizability

The above derivation of free energy, Eqs. (S2), (S3), treats each ion as a point-like charge, thus ignoring the effect of ionic polarizability, i.e. an induced dipole moment in the presence of local electric field. In the general case, this is a well known and non-trivial problem. It can be roughly accounted for by including the relative permittivity, ε, in the expression for the Coulomb energy in Eq. (S1) and below. In ScF_3, $\varepsilon \approx 2$.[22] Here, however, we include the effect of ionic polarizability directly.

First, we note that the dipolar polarizability of either Sc, or F ions does not lead to any significant correction to the Madelung energy, U_M, and therefore to the Madelung constant, M: due to high symmetry of an ideal cubic lattice of ScF_3 there is no net electric field at any site of the crystal lattice. On the other hand, transverse displacement of the F ion, $\vec{u}_\perp$, violates this symmetry requirement. This has two important consequences: (i) the displaced ion produces an electric dipole field acting on all ions of the lattice, and (ii)

there is an induced electric field at the displaced F position acting on the F ion itself. On account of finite ionic polarizability, ϑ, both of these effects lead to negative dipole contributions, which lower the net electrostatic energy of the system.

First, we consider the effect of polarization induced by the dipole electric field resulting from the fluorine displacement, $\vec{u}_\perp$, on all other ions in the lattice. The induced dipoles produce an electric field at the displaced fluorine position. In the leading order, $\sim\vec{u}_\perp^2$, the additional electrostatic energy is that of a F charge in the net dipolar field

$$\delta U_M^{(d)}(\vec{u}_\perp) = -\sum_{n,r_n\geq r} \vartheta_n\, e^2 \left(\frac{\left(1-3(\hat{a}\cdot\hat{r}_n)^2\right)}{4\pi\varepsilon_0 r_n^3}\right)^2 \frac{\vec{u}_\perp^2}{2} \approx -3N\eta\vartheta \left(\frac{e}{4\pi\varepsilon_0 r^3}\right)^2 \frac{\vec{u}_\perp^2}{2} \qquad \text{(S8)}$$

Here, ϑ_n is the polarizability of an ion at site n and the numerical coefficient, $\eta \approx 2.45$, was obtained via lattice summation, similarly to γ in Eq. (S3). Here, we adopted the value, $\vartheta_F/4\pi\varepsilon_0 = r_F^3 \approx 1.68\text{Å}^3$ ($r_F = 1.19\text{Å}$ is Fluorine ionic radius), for the F polarizability, which is consistent with the numbers reported in the literature[43]. We also use this value for the polarizability of Sc^{3+}, neglecting the small difference between the two (a similar textbook estimate gives, $\vartheta_{Sc}/4\pi\varepsilon_0 = 3r_{Sc}^3 \approx 2.08\text{Å}^3$, which is within the experimental uncertainty range[43]), thus setting $\vartheta_{Sc} \approx \vartheta_F \approx \vartheta \approx 4\pi\varepsilon_0 \cdot 1.68\text{Å}^3$. We also note that Sc sites provide only < 10% contribution to the sum in Eq. (S8).

Second, there is an electric field, $\vec{E}_F = \left(\frac{\gamma e}{4\pi\varepsilon_0 r^3} + \frac{\eta\vartheta e}{(4\pi\varepsilon_0 r^3)^2}\right)\vec{u}_\perp$, of ionic charges and induced dipoles acting on a F ion as a result of its transverse displacement, $\vec{u}_\perp$. This field gives rise to the point charge electrostatic energy described by Eqs. (S3) and (S8). On account of finite polarizability, ϑ, the displaced Fluorine ion also acquires a dipole moment, $\vec{d}_F = \vartheta\vec{E}_F$, and an additional negative dipole energy, $-\frac{1}{2}\vartheta E_F^2 \sim \vec{u}_\perp^2$, leading to

$$\delta U_M^{(p)}(\vec{u}_\perp) = -3N\frac{1}{2}\vartheta E_F^2 = -3N\vartheta\left(\frac{\gamma e}{4\pi\varepsilon_0 r^3} + \frac{\eta\vartheta e}{(4\pi\varepsilon_0 r^3)^2}\right)^2 \frac{\vec{u}_\perp^2}{2} \qquad \text{(S9)}$$

Adding the finite-polarizability contributions, Eqs. (S8), (S9), to the electrostatic energy of Eq. (S3) amounts to replacing the coefficient γ in free energy, Eqs. (S5), (S6), with $\tilde{\gamma}$

$$\tilde{\gamma} = \left(\gamma + \eta\frac{\vartheta}{4\pi\varepsilon_0 r^3}\right)\left(1 + \frac{\vartheta}{4\pi\varepsilon_0 r_0^3}\left(\gamma + \eta\frac{\vartheta}{4\pi\varepsilon_0 r^3}\right)\right) \approx 1.84 \qquad \text{(S10)}$$

On account of (S10), the NTE coefficient, Eq. (S7), becomes

$$\tilde{\alpha} = -\frac{4\pi\varepsilon_0 r_0 k_B}{(6-M-\tilde{\gamma})e^2} \approx -10.1\cdot 10^{-6}K^{-1} \qquad \text{(S11)}$$

Accounting for ionic polarizability increases the NTE effect by about a factor two, roughly consistent with the expectation based on the dielectric constant, $\varepsilon \approx 2$.[25] Finally, we note that if we use a lower value of F polarizability, $\vartheta \approx 4\pi\varepsilon_0 \cdot 1.3\text{Å}^3$, deduced from Lorenz-Lorentz analysis of the measured refraction index in fluorides[43], we obtain $\tilde{\gamma} \approx 1.57$ and $\tilde{\alpha} \approx -8.3\cdot 10^{-6}K^{-1}$. These values provide the lower bound for our estimate of the NTE effect and indicate the uncertainty range of our estimates.

Effect of finite bond rigidity: Sc-F bond expansion by entropic tension

Here, we extend our results to the case where the Sc-F bond is deformable and consider the physical mechanism leading to its positive thermal expansion, which competes with NTE. We formalize the finite rigidity of the Sc-F bond in terms of the potential energy,

$2V(r_b)$, describing the interaction of the F ion with the two nearest Sc ions, which replaces the rigid link constraint. The Sc-F bond length is now variable and temperature-dependent, $r_b = r_0 + \Delta(T)$. Here, r_0 is the equilibrium bond length at zero temperature and $r_b - r_0 = \Delta(T) \ll r_0$ is its change resulting from F thermal motion. The constraint of Eq. (S4) still holds, but now it expresses a relation between thermal averages, r_b, r, and $\langle \vec{u}_\perp^2 \rangle$, which are the variables with respect to which free energy has to be minimized. As before, we can resolve the constraint and minimize the free energy

$$F = 3N\left[-k_B T \ln(r_b^2 - r^2) + \frac{(6-M)e^2}{4\pi\varepsilon_0 r} - \frac{\gamma e^2}{4\pi\varepsilon_0 r^3}\frac{(r_b^2 - r^2)}{2} + 2V(r_b)\right] \quad \text{(S12)}$$

with respect to r_b and r to obtain the equilibrium values, $r = r(T)$, $r_b = r_b(T)$.
By minimizing the free energy of Eq. (S12) with respect to r we obtain in the leading, first order in small relative expansions, $\frac{r_b - r_0}{r_0}$, $\frac{r - r_0}{r_0}$

$$\frac{r - r_0}{r_0} - \frac{r_b - r_0}{r_0} = \frac{r - r_b}{r_0} = -\frac{4\pi\varepsilon_0 r_0 k_B T}{(6 - M - \tilde{\gamma})e^2} = \tilde{\alpha}\mathrm{T} \quad \text{(S13)}$$

This result is the same as Eq. (S7) for rigid bonds, but now the net effect of entropic tension is partitioned between the positive thermal expansion (PTE) of Sc-F bond and negative expansion of the lattice. By partially accommodating the increasing ($\sim T$) entropic tension, PTE of Sc-F bond acts to compensate NTE of the lattice, thus reducing the overall effect. The relative split of these two effects is obtained from minimization of Eq. (S12) with respect to r_b, which leads to the following condition

$$\frac{e^2 r_b}{4\pi\varepsilon_0 r^3}\left((6 - M) - 3\gamma\frac{(r_b^2 - r^2)}{2r^2}\right) = 2V_b'(r_b) \approx 2V_b'(r_0) + V_b''(r_0)(r - r_0) \quad \text{(S14)}$$

At low temperature, when $r = r_b = r_0$, this equation has a physical meaning of force balance between electrostatic repulsion and bond stretching

$$\frac{(6-M)e^2}{4\pi\varepsilon_0 r_0^2} = 2V_b'(r_0) = 2f_0 \quad \text{(S15)}$$

f_0 is the tension force provided by each Sc-F bond in order to counterbalance the net Coulomb repulsion of the remaining non-nearest neighbor ions. It is interesting to note that neutron diffraction studies under applied pressure[44] found an indication of "negative pressure" (tension) experienced by Zr-O bonds in NTE material ZrW_2O_8, which probably is of the same origin as we find here in the case of ScF_3.

In order to linearize Eq. (S14) in $\frac{r_b-r_0}{r_0}$, $\frac{r-r_0}{r_0}$, we expand the bond potential, $V_b(r_b)$, to harmonic order near the equilibrium position, $r_b = r_0$, given by Eq. (S15)

$$V_b(r_b) = V_b(r_0) + f_0(r-r_0) + \frac{1}{2}k(r-r_0)^2 + O((r-r_0)^3) \quad \text{(S16)}$$

Here, $f_0 = V_b'(r_0)$ is the tension force and $k = V_b''(r_0)$ is the effective harmonic spring constant of the Sc-F bond near the equilibrium position, Eq. (S15). Using Eqs. (S15), (S16), we obtain to the leading order

$$\frac{r_b-r_0}{r_0} = -\frac{r-r_0}{r_0}\frac{3(6-M-\tilde{\gamma})}{2\kappa-(6-M-3\tilde{\gamma})} = -\beta\frac{r-r_0}{r_0}, \text{ where } \kappa = \frac{kr_0^2}{\left(\frac{e^2}{4\pi\varepsilon_0 r_0}\right)} \quad \text{(S17)}$$

We can estimate the effective spring constant, k, from the measured frequency of the longitudinal Sc-F phonon mode, $\hbar\omega_l \approx 62$meV. We thus obtain, $2kr_0^2 = m\omega_0^2 r_0^2 \approx 51.6$eV (with $m = m_{Sc}m_F/(m_{Sc}+m_F)$, the reduced mass of Sc and F), and, using $\tilde{\gamma}$ from Eq. (S10), $\beta \approx 0.36$. This gives the relative split of Sc-F bond PTE and lattice NTE

$$\frac{r-r_0}{r_0} = \frac{\tilde{\alpha}}{1+\beta}T \approx -7.4\cdot 10^{-6}T \quad \text{(S18)}$$

$$\frac{r_b-r_0}{r_0} = \frac{\tilde{\alpha}\beta}{1+\beta}T \approx 2.7\cdot 10^{-6}T \quad \text{(S19)}$$

We conclude that floppy vibration modes associated with transverse fluorine displacement in an under-constrained ScF_3 crystal structure give rise to both negative

expansion of the lattice and positive expansion of Sc-F bond. The latter effect is distinct from the conventional positive thermal expansion based on cubic anharmonicity of the Sc-F bond potential, $V_b(r_b)$. Instead, it originates from entropic anharmonicity via floppy modes and is already present for the harmonic Sc-F bond, Eq. (S16). Finally, we note, that in the absence of F transverse displacement conventional PTE based on cubic anharmonicity of Sc-F potential is suppressed in ScF_3 as a result of symmetric position of F ion in-between the two Sc: the potential energy of its interaction with two nearest Sc neighbors is symmetric with respect to the equilibrium position.

The effective Hamiltonian and dynamics of floppy modes in ScF_3

The transverse motion of each F ion in the floppy network model of ScF_3 is decoupled from the other ions thanks to the under-constrained nature (floppiness) of the lattice. In the absence of negative pressure (tension) provided by the electrostatic Coulomb repulsion of like-charged ions, transverse (floppy) F vibration modes have zero energy and the lattice is unstable. The electrostatic repulsion provides tension (negative pressure), which balances entropic elasticity of the network and stabilizes the lattice. On the mean field level, transverse F vibrations are still local, decoupled from the rest of the lattice, but now have finite energy, E_t. Such an MF-RPA approximation neglects the dependence of Coulomb electrostatic energy on the correlation between displacements of different ions. Consequently, transverse F vibrations appear as local, dispersionless Einstein phonon modes. At low enough temperatures, these vibrations are frozen out and such an approximation could be unsatisfactory, similarly to Einstein's model for heat capacity. In this case, accounting for the realistic low-energy phonon dispersions obtained by going beyond an MF-RPA approximation is required, such as in Debye theory. However, the difference vanishes at high enough temperature, where the transverse fluctuations of F ions are all thermally excited and the corresponding degrees of freedom are equipartitioned. This is similar to the vanishing difference between Einstein and Debye models for heat capacity at high enough temperatures, which both converge to the Dulong-Petit law. The exact form of the phonon dispersion curves does not matter in this regime, where vibrational degrees of freedom are equipartitioned. The approximation adopted in our entropic elasticity model of the floppy network in ScF_3,

Eqs. (S2), (S12) is, strictly speaking, only justified in such an equipartitioning regime, at temperatures $T > E_t/k_B$ ($E_t = h\nu_t$ is the energy of the F floppy modes, where ν_t is the frequency and h is the Planck constant). Here, we evaluate E_t, thus verifying the consistency of our description.

In order to evaluate the range of applicability of our entropic MF approximation, we derive the effective Hamiltonian for transverse fluorine motion and obtain the resulting phonon energy of the floppy vibration modes. Let $\vec{u}_{i\perp}$ be the transverse displacement of a F ion at site i. In terms of these local coordinates, $\vec{u}_{i\perp}$, the Hamiltonian describing fluorine motion can be written as

$$H = K + \frac{3N(6-M)e^2}{4\pi\varepsilon_0 r} - \sum_i \frac{\gamma e^2}{4\pi\varepsilon_0 r^3}\frac{\vec{u}_{i\perp}^2}{2} \qquad \text{(S20)}$$

The Sc-F average distance, r_b, the variable average lattice repeat parameter, $2r$, and floppy mode coordinates, $\vec{u}_{i,\perp}$, obey an exact geometric relation

$$\sum_i (r_b^2 - r^2 - \vec{u}_{i\perp}^2) = 0 \qquad \text{(S21)}$$

which replaces the averaged constraint of Eq. (S4), or its linearized version. In considering dynamics of the floppy modes we neglect finite longitudinal bond rigidity, setting $r_b = r_0$. Accounting for the constraint, Eq. (S21), while calculating the partition function leads to the following expression for the free energy of the system

$$F = -k_B T \ln\left(\int D\{\vec{u}_{i\perp}, \vec{p}_{i\perp}\}\, e^{-\frac{H}{k_B T}} \delta\left(\sum_i (r_0^2 - r^2 - \vec{u}_{i\perp}^2)\right)\right) =$$

$$-k_B T \ln\left(\int_{-i\infty}^{i\infty} \frac{df}{2\pi k_B T} \int D\{\vec{u}_{i\perp}, \vec{p}_{i\perp}\}\, e^{-\frac{\tilde{H}}{k_B T}} \right) \quad \text{(S22)}$$

Here, $\int D\{\vec{u}_{i\perp}, \vec{p}_{i\perp}\}$ represents an integration over the coordinates and momenta of the floppy modes, and δ-function was exponentiated in a standard way, by introducing a fictitious variable, f, conjugated to the constraint. This leads to an addition of a Lagrange multiplier term, $-\frac{f}{2r_0}\sum_i (r_0^2 - r^2 - \vec{u}_{i\perp}^2)$, to the original Hamiltonian, Eq. (S20), which now becomes

$$\tilde{H} = K + \frac{3N(6-M)e^2}{4\pi\varepsilon_0 r} - 3N\frac{f}{2r_0}(r_0^2 - r^2) + \sum_i \left(\frac{f}{r_0} - \frac{\gamma e^2}{4\pi\varepsilon_0 r^3}\right)\frac{\vec{u}_{i\perp}^2}{2} \quad \text{(S23)}$$

The physical meaning of the variable f is that it represents the tension force applied to each Sc-F bond due to the net electrostatic repulsion of all other ions. Minimization of the potential energy in the Hamiltonian, Eq. (S23), with respect to r yields the value of this force

$$f = \frac{(6-M)e^2}{4\pi\varepsilon_0 r^2}\frac{r_0}{r} \approx \frac{(6-M)e^2}{4\pi\varepsilon_0 r_0^2} \quad \text{(S24)}$$

Here, replacing r with r_0 we neglect terms of the order $\frac{r_0 - r}{r_0} \sim \frac{\langle \vec{u}_1^2 \rangle}{r_0^2}$. Minimization of the Hamiltonian with respect to f reproduces the original constraint, Eq. (S21).

We thus obtain an oscillator Hamiltonian of the F floppy modes, which is the part of Eq. (S23) that is quadratic in transverse displacements and momenta (m_F is mass of F ion)

$$H_\perp = K + \sum_i \left(\frac{f}{r_0} - \frac{\gamma e^2}{4\pi\varepsilon_0 r^3}\right)\frac{\vec{u}_{i\perp}^2}{2} \approx \sum_i \left(\frac{\vec{p}_{i\perp}^2}{2m_F} + \frac{(6-M-\gamma)e^2}{4\pi\varepsilon_0 r_0^3}\frac{\vec{u}_{i\perp}^2}{2}\right) \quad \text{(S25)}$$

Since in the MF approximation we have neglected the coupling between displacements of different F ions, all the modes have the same frequency rendered by the tension effect, which sets the energy scale for the soft floppy phonons in the system

$$\hbar\omega_0 = \hbar e\sqrt{\frac{(6-M-\widetilde{\gamma})}{4\pi\varepsilon_0 r_0^3 m_F}} \approx 21.6 \text{ meV} \quad \text{(S26)}$$

This value compares very favorably with the phonon dispersions measured in ScF_3, where low-energy peaks in the density of states corresponding to transverse F vibrations are observed below ≈ 22 meV. In the classical regime, i.e. when $k_B T > \hbar\omega_0$, the equipartition theorem sets the thermal averages of the potential and kinetic energy terms in the above Hamiltonian to $k_B T/2$ per degree of freedom. This leads to the previously derived result for NTE, Eq. (S13), which is thus applicable for $T \gtrsim 250$ K.

Since each of the modes in our MF approximation has a Hamiltonian of an oscillator with frequency ω_0, the value of $\langle\vec{u}_\perp^2\rangle = \langle\vec{u}_{i\perp}^2\rangle$ can be found with full account for quantum effects and for an arbitrary temperature

$$\frac{r-r_0}{r_0} \approx -\frac{\langle\vec{u}_\perp^2\rangle - \langle\vec{u}_\perp^2\rangle_0}{2r_0^2} = -\alpha T\left[\frac{\hbar\omega_0}{k_B T}\left(e^{\frac{\hbar\omega_0}{k_B T}} - 1\right)^{-1}\right] \quad \text{(S27)}$$

Here, $\langle \vec{u}_{\perp}^{2} \rangle_0$ represents the contribution from zero-point oscillations, which we incorporate in r_0, by re-defining, $r_0 \rightarrow r_0 - \frac{\langle \vec{u}_{\perp}^{2} \rangle_0}{2r_0}$.

The Sc-F bond and Coulomb energy in ScF_3

The nature of bond rigidity in ScF_3: "hidden" covalency

The exceptional rigidity of the Sc-F bond, which underpins the NTE effect in ScF_3, is rather remarkable and it is important to understand its nature. Here, we review the experimental evidence, which suggests that it is borne out by "hidden" covalency, where a very small degree of hybridization and charge transfer between F and Sc ions, insignificant in terms of inter-ionic Coulomb energy, causes substantial energy gain stabilizing the Sc-F bond. The physical origin of this effect is that the highest occupied F 2p, F 2s and Sc 3p atomic orbitals are very compact and have energies that lie rather deep, 4 eV to 30 eV below the Fermi level[25,45]. By the virial theorem, this energy determines the kinetic energy of electrons in these atomic orbitals. Hence, a large gain in kinetic energy is possible if electrons in such an orbital, lying far below Fermi level delocalize via orbital hybridization with a neighbor ion. Similar ideas were recently discussed in terms of the new type of chemical bond, the charge transfer bond, which was introduced to describe Lewis type dative covalent bonding[46].

The nature of bonding (ionic vs covalent) in binary fluorine complexes is a topic with a long and venerable history, which continues to attract significant attention[23,25,27,46-50]. The propensity of fluorine to forming strong bonds is well documented: according to the bond dissociation energy[23] covalent Si-F and C-F bonds are among the strongest single bonds occurring in nature. However, because F has the highest electronegativity of all elements[23,48,49], fluorine bonds are usually highly polar and therefore have significant ionic component, which obscures covalent nature. It is generally accepted that covalent bonding is dominant in binary fluorides of non-metallic main group elements, such as BF_3, PF_3, CF_4, SiF_4, SF_6, which under normal conditions are in the gaseous phase[46,47], even though strong ionic polarization, of the Si-F bond for example, is not dissimilar to $Na^+ – Cl^-$ in NaCl, which is a prime example of ionic bonding[23,46-48].

Metal trihalides, MX_3 (M = Al, Sc, Fe, In, …, X = F, Cl, Br, I), are usually considered to be ionic compounds[31,37] due to the very high degree of polarization of M^{3+} and X^- ions (using Pauling's electronegativity estimate we obtain, $\delta \approx 1 - e^{0.25(\chi_F - \chi_{Sc})^2} \approx 0.84$ for a single Sc-F bond[46]). But ScF_3 was early on found to be a notable irregularity in this series[31]. Indeed, ionic bonding implies regular dependence of the bond energy on the difference of electronegativity and ionic radii of M^{3+} and X^- species. It was observed, however, that the scandium fluoride complexes are markedly more stable than those of other trivalent ions of comparable radius and that the extra stability arises from an irregularity in the enthalpy, rather than in the entropy term. Thus, ScF_3 having a roughly 2 eV stronger bond compared to similar Al, Fe and In fluoride compounds presents a remarkable exception from the regularity expected in the ionic picture[27]. If one assumes the fluoride complexes to be purely ionic, which putatively seems to be a reasonable assumption due to low polarizability of the fluoride ion, one would expect the scandium complexes to be stronger than those of indium, but weaker than those of iron and aluminium, contrary to what is observed. Nevertheless, at the time, authors shied from accepting the "hidden" covalency and argued that "the relatively greater stability of the scandium fluoride complex is almost certainly not due to covalent bond formation since such ions as Fe^{3+} and In^{3+} would be expected to deviate even further, and they do not", concluding that "the reason for this degree of failure of the simple ionic model is not clear"[31].

ScF_3 is also anomalous in the ScX_3 halide series. In all four halides, which under normal conditions form solids, the scandium is 6-coordinated[46]. For X= Cl, Br, or I, these halides are very soluble in water, while ScF_3 is insoluble. Moreover, in a solution containing excess fluoride ion it dissolves to form octahedrally coordinated $[ScF_6]^{3-}$ anion, similar in structure to the supervalent compound, SF_6.[50] Such behavior is typical of a Lewis acid, such as boron trifluoride, BF_3, which can accept a pair of electrons donated by fluoride ion, forming a dative covalent bond, $BF_3 + F^- \rightarrow [BF_4]^-$. The above observations provide strong indication of covalent bonding in the ScF_3 complex.

The nature of the hidden covalency in ScF_3 has been perhaps most clearly revealed by X-ray photoelectron spectroscopy (XPS) studies combined with the Density Functional

Theory (DFT) analysis of the electronic structure of Sc-F molecular clusters[25]. The analysis of fine structure in the XPS spectra indicates a non-negligible dp hybridization of certain outer valence molecular orbitals (OMVO) and a ps hybridization of inner valence molecular orbitals (IMVO) lying deep below the Fermi level, at -5 eV to -30 eV. Even a small hybridization of such deep atomic orbitals can lead to a large energy change and therefore significantly contribute to the covalent bonding between scandium and fluorine. The results of the investigations into the nature of the chemical bond formation in the $[ScF_6]^{3-}$ cluster (C3 symmetry) imply that the greatest contribution to its stability is made by the 5a1 [16(Sc3d)+83(F2p)] OVMO (-1.42 eV) and 2a1 Sc3p-F2s [4(Sc3p)+95(F2s)] and 1a1 Sc3p-F2s [3(Sc3p)+96(F2s)] IVMO (-0.67 eV and -0.4 eV, respectively) electrons. We note that with only few percent mixing, covalent bond formation of the Sc3p-F2s (2a1 and 1a1) IVMO provides strong binding between the neighboring atoms and accounts for $\approx 43\%$ of the total covalent contribution of ≈ -2.5 eV to the chemical bond energy. It thus appears highly likely that the charge transfer bonding of deep atomic orbitals, which is non-directional and is not accompanied by a significant charge transfer, is at the origin of the hidden covalency that renders exceptional longitudinal rigidity to Sc-F bond in ScF_3.

Table S1. Scandium ionization energies, E_i(Sc) (*45*), and fluorine electron affinity, E_a(F) (*49*), used in eq. S28.

Unit	E_a(F)	E_1(Sc)	E_2(Sc)	E_3(Sc)	E_4(Sc)
kJ/mol	328.1649	633.1	1235.0	2388.6	7090.6
eV	3.401189	6.5615	12.79967	24.75666	73.4894

Madelung sum and Coulomb energy in ScF_3 crystal

In order to understand the nature of chemical bonding in ScF_3, it is useful to consider the contribution of ionic bonding to its cohesion energy, as well as to the energy of an octahedral ScF_6 cluster, which can be viewed as the molecular building block of its

crystal structure. The ionic contribution to the bonding energy of ScF_3 molecular unit can be estimated by balancing scandium ionization energy, $E_i(Sc)$ ($i = 1,2,3$), with fluorine electron affinity, $E_a(F)$, and the ionic Coulomb interaction, E_C,[46,47]

$$E_{ionic} \approx \sum_{i=1}^{3} E_i(Sc) - 3E_a(F) - 3M_{ScF_3} \frac{e^2}{4\pi\varepsilon_0 r_{Sc-F}} \left(1 - \frac{1}{n}\right) \quad \text{(S28)}$$

Here, M_{ScF_3} is the effective Madelung constant for ScF_3 molecule, $r_{Sc-F} \approx 2$Å is the Sc-F equilibrium distance in the ScF_3 crystal structure, and $n \approx 10$ is the exponent of the Born-Lande repulsive interaction, which is one possible choice of a phenomenological short-range repulsive potential that needs to be added to the inter-ionic attractive Coulomb interaction in order to stabilize an ionic bond. From Table S1

$$\sum_{i=1}^{3} E_i(Sc) - 3E_a(F) \approx 33.9 \text{ eV} \quad \text{(S29)}$$

The Madelung constant for a crystal is defined to parameterize the sum of Coulomb interactions between ions, which are treated as point charges, in terms of the characteristic distance in a lattice, a

$$E_C = \frac{1}{2}\sum_{i,j} \frac{Z_i Z_j e^2}{4\pi\varepsilon_0 r_{ij}} = M_a \frac{e^2}{4\pi\varepsilon_0 a} \quad \text{(S30)}$$

Here, i and j index ions on the lattice, their charges are $Z_i e$ and $Z_j e$, respectively, and 1/2 accounts for double counting of each pair in the sum, as in Eq. (S1). Index in M_a indicates that, depending on the convention, a can be either the shortest anion-cation distance, or the unit cell parameter of a cubic or pseudo-cubic lattice[41]. Here, we define Madelung constant for ScF_3 with respect to Sc-F bond length, in line with the definition

for molecular clusters, Eq. (S30). We further normalize M per number of F ions in crystal unit cell. With this definition, we obtain $3M \approx 8.95$,[42] which, accounting for the difference in definition agrees with the previously published value (the published M was determined with respect to the lattice repeat, $a = 2r_{Sc-F}$, and so is twice larger)[40].

In our approach, we consider the interaction between the nearest-neighbor Sc and F ions separately from the rest of ionic pairs, because in addition to Coulomb attraction it also contains contributions from core repulsion and covalent bonding via molecular orbital (MO) formation. The net Coulomb energy without accounting for the Sc-F bonds is positive: $E_C = \frac{(6-M)e^2}{4\pi\varepsilon_0 r}$. The Coulomb interaction beyond the nearest neighbors increases the electrostatic energy, reducing the energy gain from the nearest-neighbor attraction roughly by factor 2. It thus corresponds to a net repulsion that creates negative pressure. The energy of the ionic nearest neighbor Coulomb attraction is, $-\frac{1}{6}\frac{3Me^2}{4\pi\varepsilon_0 r} \approx -10.7$ eV per Sc-F bond. If we account for the balance of Sc ionization and F electron affinity energies, the net ionic contribution to Sc-F bonding energy in ScF_3 crystal is

$$E_{ionic,cryst} \approx \sum_{i=1}^{3} E_i(Sc) - 3E_a(F) - 3M\frac{e^2}{4\pi\varepsilon_0} \approx -30.4 \text{ eV} \qquad \text{(S31)}$$

Distributing this energy among 6 Sc-F bonds per Sc ion, we obtain ≈ -5 eV per bond, which is comparable with the covalent contribution to the energy of the Sc-F bond. This energy is also close to the estimate obtained from Pauling's relation between the ionic bonding energy and the electronegativity[46], $E_{ionic\ bond} \approx -23.06(\chi_F - \chi_{Sc})^2 \approx -7.3$ eV, where $\chi_F \approx 4$ and $\chi_{Sc} \approx 1.3$ are F and Sc electronegativities, respectively[48].

DFT results

In order to understand the degree of Sc-F hybridization and the effective potential of the F ion in the ScF_3 crystal, we carried out the first principles density functional theory

(DFT) calculations of the electronic band structure (Fig. S1). The DFT calculations were performed using the full electron scheme with the generalized gradient approximation as implemented in WIEN2k[51-53]. The maximally localized Wannier functions were then computed using the wannier90 code[51-53] and the Wien2Wannier interface[54]. The band structure of the tight-binding model derived from the Wannier functions captures the band structure from density functional calculations quite well.

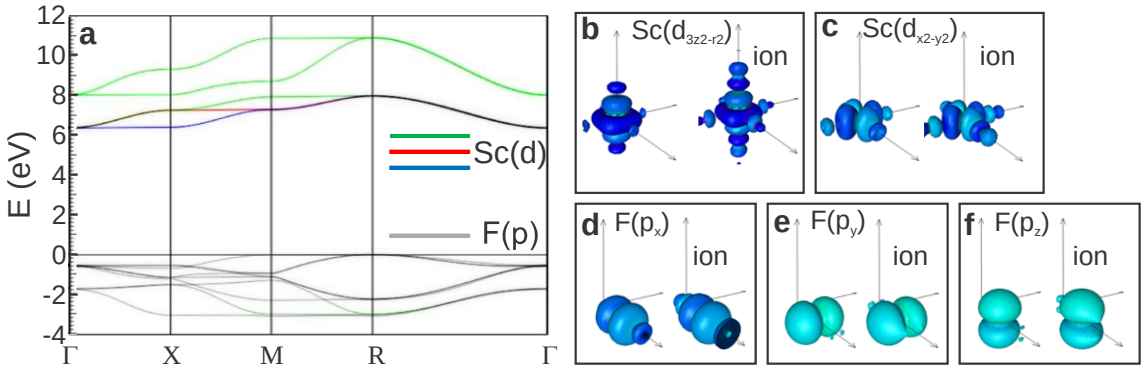

Fig. S1. Electronic band structure in ScF_3. The orbital-resolved DFT band structure, (**a**): F(p) character is shown in grey, Sc($d_{3z^2-r^2}$, $d_{x^2-y^2}$, d_{xy}) in green, Sc(d_{xz}) in blue, and Sc(d_{yz}) in red. A slight admixture of green in the low-lying filled, (Fp)-derived valence band below -3 eV indicates Sc-F, d-p hybridization. The Sc- and F-centered, bonding Sc($d_{3z^2-r^2}$), Sc($d_{x^2-y^2}$), (**b**), (**c**) and F(p_x), F(p_y), and F(p_z), (**d**) – (**f**), Wannier orbitals, respectively, are shown on the left in each panel. On the right, the corresponding orbital (marked "ion") is shown in the absence of Sc-F hopping term. A very slight decrease in the size of the actual orbital in the presence of hopping indicates some charge transfer by hybridization.

The orbital-resolved electronic band structure along high-symmetry directions of the Brillioun zone is shown in Fig. S1a. Overall, the band structure agrees with the local density approximation (LDA) results[55], where authors also find small Sc(d) contribution to the density of states in the highest filled F(p) valence band, as well as an evidence for Sc(p)-F(s) hybridization in the deep valence band near -20 eV. Using modified hybrid

exchange-correlation functionals, or GW approximation (G is the Green's function and W the screened Coulomb interaction) within the DFT yields a similar spectrum, but with all energies scaled upward to give an about 30% larger band gap.[26,55] Although in Ref. 26 authors do not show the orbitally resolved band structure, they have analyzed the effective charges of scandium and fluorine atoms obtained from *ab initio* calculations using the linear combination of atomic orbital (LCAO) and plane wave projector augmented-wave (PAW) methods. Despite quantitative scatter depending on the method, from $Sc^{+2.28}(F^{-0.76})_3$ in LCAO to $Sc^{+2.17}(F^{-0.73})_3$ and $Sc^{+2.7}(F^{-0.9})_3$ in PAW, depending on Sc pseudopotential used, the results demonstrate considerable deviations from formal ionic charges caused by the partly covalent nature of the Sc-F bonds (using Pauling's electronegativity estimate[46] we obtained $F^{-0.84}$). We note, that the decrease of fluorine ionic charge, q_{eff}, leads to the decrease of Coulomb interactions and the Madelung energy, which scale down $\sim q_{eff}^2$ and thus increases the NTE effect, which is inversely proportional to q_{eff}^2, Eqs. (S7), (S11). For $F^{-0.84}$, this is an ≈ 30% increase.

Table S2. Frozen phonon calculation of the energy change as a function of the longitudinal ($\Delta E_{\parallel}$) and transverse ($\Delta E_{\perp}$) fluorine displacement in ScF_3. The total energy, E_0 = -28959.5 eV, the lattice constant, a= 4.01Å.

Displacement (Å)	$\Delta E_{\parallel}$ (eV)	$\Delta E_{\perp}$ (eV)
0.4 (10%)	1.4985	0.1295
0.2 (5%)	0.2304	0.0279
0.1 (2.5%)	0.0271	0.0064

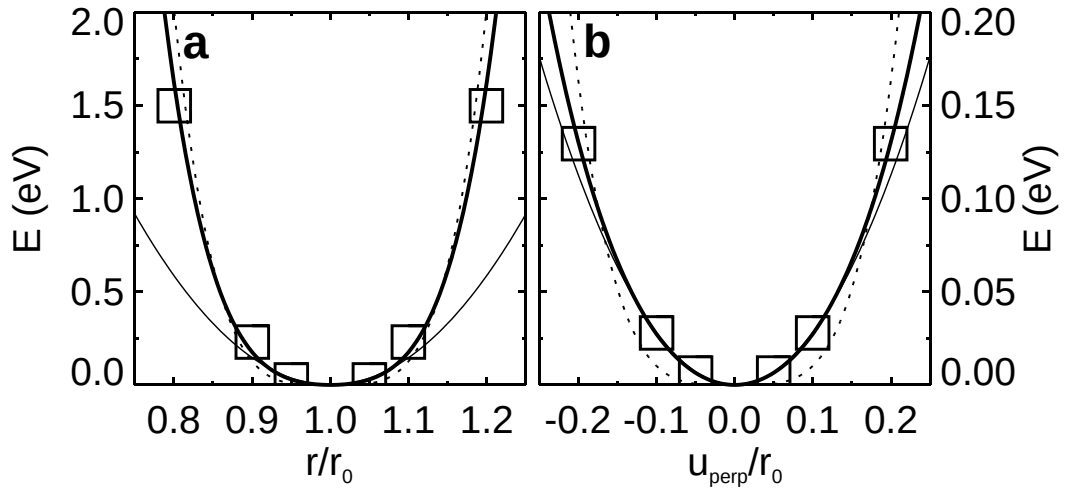

Fig. S2. Effective potential of the fluorine ion in ScF_3. The energy change obtained in frozen phonon calculation as a function of longitudinal (**a**) and transverse (**b**) displacement of the fluorine ion. The thin solid line is the best fit by harmonic quadratic potential, $U(x) = \frac{1}{2} k\, x^2$, dotted by quartic, $U(x) = \frac{1}{4} k_4 x^4$, and the thick solid line is the best fit by the harmonic plus the quartic anharmonic term, $U(x) = \frac{1}{2} k\, x^2 + \frac{1}{4} k_4 x^4$. The parameters of these fits are listed in table S2.

We further performed the effective bond potential analysis by carrying out the frozen phonon calculations. The change in energy corresponding to displacement of the F ion by 2.5%, 5% and 10% of lattice spacing either along or perpendicular to the nominal Sc-F bond direction was computed and modelled by an effective anharmonic potential, $U(x) = \frac{1}{2} k\, x^2 + \frac{1}{4} k_4 x^4$. The results are presented in Table S2 and Figure S2. The calculation confirms that the longitudinal potential, $U_{\parallel}(x)$, is more than an order of magnitude stronger than the potential for the transverse displacement, $U_{\perp}(x)$, supporting the energy scale separation scenario. Although the analysis of harmonic vs anharmonic terms based on these results is tentative at most, it provides several interesting indications. The chi-squared (based on a 10% error of the calculated energy) shown in the last column of Table S2 suggests that transverse displacement potential, albeit weak, is only very slightly anharmonic. This is at variance with the naïve expectation of quartic potential arising from the longitudinal harmonic bond tension proposed previously[17]. On the other hand, this agrees well with the Coulomb returning potential of Eq. (S25),

$U(x) = \frac{1}{2} k\, x^2$ with $k \approx 8.5$eV, which is to be compared to $k \approx 5.6$ eV in Table S2. The ≈ 30% difference is consistent with the underestimate of the band gap in LDA and can be further reduced if covalent reduction of the F ionic charge is taken into account. The longitudinal bond potential, on the contrary, is very anharmonic, with quartic contribution nearly dominant (Fig. S2a). This is consistent with large contribution from covalent bonding.

Table S3. Parameters of an effective potential, $\boldsymbol{U(x) = \frac{1}{2} kx^2 + \frac{1}{4} k_4 x^4}$, for the longitudinal, $\boldsymbol{U_{\parallel}\left(\frac{r-r_0}{r_0}\right)}$, and transverse, $\boldsymbol{U_{\perp}\left(\frac{u_{\perp}}{r_0}\right)}$, $\boldsymbol{r_0 = 2.0}$Å fluorine displacement in $\boldsymbol{ScF_3}$. Last column shows the corresponding chi-squared.

Potential	k (eV)	k_4 (eV)	χ^2
$U_{\parallel}(x)$	29.38	0	25.0
$U_{\parallel}(x)$	0	5065.8	33.1
$U_{\parallel}(x)$	19.92	3076.8	3.57
$U_{\perp}(x)$	5.64	0	1.08
$U_{\perp}(x)$	0	410.5	51.2
$U_{\perp}(x)$	5.14	70.3	0.04

Supplementary neutron scattering data

Rietveld refinement results

In our model presented in Figs. 3a and 4a of the main text, we use the Gaussian atomic displacement parameters (ADPs) derived by Rietveld analysis of Bragg diffraction for setting up the ring and the toroidal model. These ADPs adequately quantify the atomic mean square displacement. Our model is therefore set up by matching the mean square displacement of the model (which is given by the radius of the ring, or torus) to that obtained from Rietveld analysis. The idea behind this choice is that a Gaussian adequately captures mean square deviation even for non-Gaussian distributions. The parameters refined by Rietveld analysis of NOMAD and NPDF data are listed in Tables

S4 and S5, respectively. The representative diffraction patterns together with Rietveld fits are shown in Fig. S3.

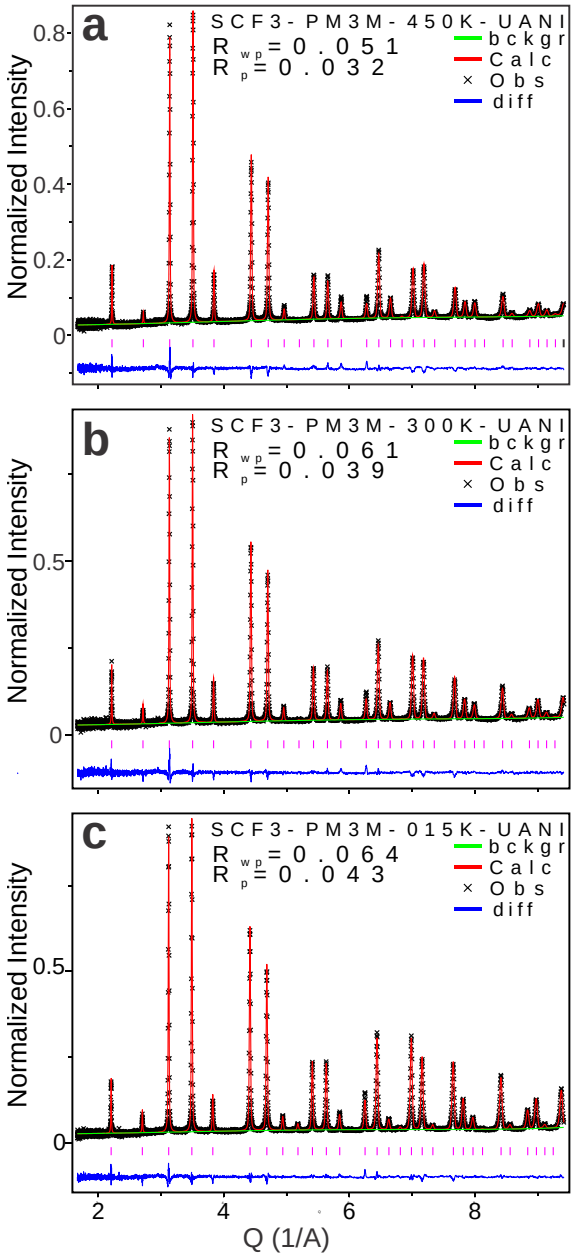

Fig. S3. Selected plots of Rietveld refinement of structural parameters in ScF_3. The typical diffraction patterns measured at NPDF (detector bank #2) at 450K (**a**), 300K (**b**) and 15K (**c**). The structural parameters obtained from these refinements including the anisotropic displacement parameters are listed in table S4.

We have carried out similar model analysis using the experimental Sc-F and LRD distances obtained from fits of PDF peaks in Fig. 2 of main text instead of Rietveld results. While this analysis provides very similar agreemen, for temperatures below about 200 K the scatter of the LRD and Sc-F peak positions refined from PDF peaks is too large and for some temperatures the refined positions do not satisfy the triangle inequality (note that the peak position needs to be refined with accuracy better than 1% of peak FWHM). For this reason, we selected the model using the Rietveld parameters shown in Tables S4 and S5 for the presentation in main text.

Table S4. The structural parameters of ScF_3 obtained from Rietveld refinements of NOMAD data showing the standard uncertainty for the lattice spacing, *a* (measured in Å), and the atomic mean square displacement parameters (measured in 0.01*Å^2), isotropic for Sc ($U_{iso\text{-}Sc}$) and anisotropic for F ($U_{par\text{-}F}$ and $U_{perp\text{-}F}$, both measured in 0.01*Å^2).

T(K)	a	Δa	$U_{iso\text{-}Sc}$	$\Delta U_{iso\text{-}Sc}$	$U_{par\text{-}F}$	$\Delta U_{par\text{-}F}$	$U_{perp\text{-}F}$	$\Delta U_{perp\text{-}F}$
2	4.0271	0.0001	0.19	0.02	0.09	0.06	0.77	0.05
4	4.0271	0.0001	0.21	0.02	0.09	0.06	0.72	0.05
6	4.0271	0.0001	0.20	0.02	0.09	0.06	0.80	0.05
8	4.0271	0.0001	0.19	0.02	0.09	0.06	0.74	0.05
10	4.0271	0.0001	0.20	0.02	0.09	0.06	0.79	0.05
12	4.0271	0.0001	0.20	0.02	0.09	0.06	0.78	0.05
14	4.0271	0.0001	0.19	0.02	0.09	0.06	0.80	0.05
16	4.0271	0.0001	0.21	0.02	0.09	0.06	0.75	0.05
18	4.0270	0.0001	0.19	0.02	0.09	0.06	0.78	0.05
20	4.0270	0.0001	0.22	0.02	0.09	0.06	0.81	0.05
22	4.0270	0.0001	0.22	0.02	0.09	0.06	0.82	0.05
24	4.0269	0.0001	0.23	0.02	0.09	0.06	0.84	0.05
50	4.0262	0.0001	0.22	0.02	0.10	0.06	0.90	0.05
75	4.0250	0.0001	0.23	0.03	0.11	0.10	0.99	0.10
100	4.0238	0.0001	0.24	0.03	0.12	0.10	1.20	0.10
125	4.0235	0.0001	0.27	0.02	0.12	0.07	1.29	0.05

150	4.0228	0.0001	0.30	0.02	0.13	0.07	1.38	0.05
175	4.0219	0.0001	0.33	0.02	0.13	0.07	1.48	0.05
200	4.0210	0.0001	0.38	0.02	0.14	0.07	1.75	0.05
225	4.0200	0.0001	0.44	0.02	0.14	0.07	1.85	0.06
250	4.0192	0.0001	0.47	0.02	0.15	0.07	2.12	0.06
275	4.0177	0.0001	0.48	0.02	0.15	0.07	2.34	0.06
300	4.0130	0.0001	0.55	0.02	0.13	0.07	2.74	0.07
400	4.0098	0.0001	0.79	0.02	0.31	0.07	3.79	0.07
433	4.0091	0.0001	0.87	0.02	0.35	0.07	4.11	0.07
466	4.0085	0.0001	0.92	0.02	0.38	0.07	4.36	0.07
500	4.0079	0.0001	0.98	0.02	0.44	0.07	4.61	0.07
533	4.0074	0.0001	1.05	0.03	0.45	0.07	4.89	0.08
566	4.0069	0.0001	1.12	0.03	0.53	0.07	5.18	0.08
600	4.0066	0.0001	1.16	0.03	0.60	0.07	5.40	0.08
633	4.0061	0.0001	1.26	0.03	0.63	0.07	5.69	0.08
666	4.0058	0.0001	1.30	0.03	0.67	0.07	5.94	0.08
700	4.0054	0.0001	1.37	0.03	0.74	0.07	6.17	0.09
733	4.0052	0.0001	1.44	0.03	0.79	0.07	6.42	0.09
766	4.0049	0.0001	1.51	0.03	0.87	0.07	6.69	0.10
800	4.0047	0.0001	1.56	0.03	0.91	0.07	6.88	0.10
833	4.0044	0.0001	1.64	0.03	0.92	0.07	7.18	0.11
866	4.0043	0.0001	1.70	0.03	1.03	0.07	7.35	0.11
900	4.0041	0.0001	1.77	0.03	1.15	0.07	7.54	0.12
933	4.0039	0.0001	1.64	0.04	1.00	0.08	7.71	0.13
966	4.0038	0.0001	1.91	0.04	1.27	0.08	8.06	0.13
1000	4.0037	0.0001	2.01	0.04	1.31	0.08	8.36	0.14
1033	4.0037	0.0001	2.10	0.04	1.40	0.08	8.55	0.15
1066	4.0037	0.0001	2.28	0.04	1.49	0.10	8.85	0.17
1100	4.0037	0.0001	2.22	0.04	1.50	0.10	9.08	0.17
1133	4.0037	0.0001	2.29	0.04	1.58	0.10	9.30	0.17

1166	4.0036	0.0001	2.33	0.05	1.72	0.10	9.42	0.18
1200	4.0036	0.0001	2.20	0.05	1.53	0.10	9.68	0.19
1233	4.0036	0.0001	2.21	0.05	1.66	0.10	9.75	0.19
1266	4.0037	0.0001	2.57	0.05	1.98	0.11	10.4	0.21

Table S5. The structural parameters of ScF_3 obtained from Rietveld refinements of NPDF data including parameters R_{wp} and R_p quantifying the goodness of the fit.

T(K)	a (Å)	V (Å^3)	r_{Sc-F} (Å)	r_{F-F} (Å)	U_{iso-Sc} (Å^2)	U_{par-F} (Å^2)	U_{perp-F} (Å^2)	R_{wp}	R_p
15	4.023406	65.130	2.01170	2.84498	0.00388	0.00178	0.00937	0.0643	0.0433
30	4.023112	65.116	2.01156	2.84477	0.00390	0.00172	0.00974	0.0637	0.0432
50	4.022432	65.083	2.01122	2.84429	0.00403	0.00180	0.0107	0.0626	0.0425
75	4.021271	65.026	2.01064	2.84347	0.00436	0.00199	0.01245	0.0610	0.0413
100	4.020126	64.971	2.01006	2.84266	0.00460	0.00195	0.01417	0.0602	0.0405
150	4.017839	64.860	2.00892	2.84104	0.00533	0.00225	0.01816	0.0582	0.0389
200	4.015949	64.769	2.00797	2.8397	0.00613	0.00257	0.02214	0.0565	0.0378
300	4.012788	64.616	2.00639	2.83747	0.00789	0.00327	0.02983	0.0608	0.0391
375	4.009817	64.472	2.00491	2.83537	0.01008	0.00464	0.03998	0.0513	0.0336
450	4.008085	64.389	2.00404	2.83414	0.01197	0.00544	0.04697	0.0511	0.0325